



Non-aeolian sand ripples

To cite this article: J. F. Boudet *et al* 2005 *EPL* **69** 365

View the [article online](#) for updates and enhancements.

You may also like

- [Special issue on applied neurodynamics: from neural dynamics to neural engineering](#)
Hillel J Chiel and Peter J Thomas
- [SciDAC 2009](#)
Michael Strayer
- [Workshop on Intakes of Radionuclides: Occupational and Public Exposure, Avignon, 15-18 September 1997](#)
G Etherington, A W Phipps, J D Harrison et al.

Non-aeolian sand ripples

J. F. BOUDET, Y. AMAROUCHENE, B. BONNIER and H. KELLAY
*CPMOH (UMR5798), U. Bordeaux 1 - 351 cours de la Libération
33405 Talence, France*

received 1 September 2004; accepted in final form 24 November 2004
published online 24 December 2004

PACS. 45.70.-n – Granular systems.

PACS. 45.70.Ht – Avalanches.

PACS. 45.70.Qj – Pattern formation.

Abstract. – By examining the initial stages of the impact of a granular jet on a flat horizontal solid surface we evidenced the existence of oscillatory sand fronts. These oscillations give rise to a novel mechanism for the formation of ripples on sand surfaces. We here show that as the front advances, its slope changes periodically in time, leaving behind a succession of surface elevations and depressions. A key feature of these oscillations is the interplay between the deposition of mobile sand and the avalanching of the static parts giving rise to a remarkable self-regulating system. These features come out naturally from a simplified version of recently proposed models for the dynamics of sand piles.

The dynamics of granular materials is complex and may lead to the formation of different types of patterns such as sand dunes and sand ripples [1]. These materials exhibit a behavior that crosses the frontiers between different states of matter [2, 3]. Certain experiments display liquid-like properties [4], while others show solid-like behavior and clustering even under continuous mechanical agitation [3, 5]. Such diversity in possible states renders a continuum description of these materials very difficult. Another difficult aspect is the existence of sand fronts which are sharp regions separating flowing and static sand. Understanding the dynamics of such fronts is believed to be of central importance in the modeling of the dynamics of granular materials [6, 7]. Here, by examining the initial stages of the impact of a granular jet on a flat horizontal solid surface we evidenced the existence of oscillatory sand fronts: as the front advances, its slope changes periodically in time, leaving behind a succession of surface elevations and depressions. These oscillations give rise to a novel mechanism for the formation of ripples on sand surfaces and come out naturally from a simplified version of recently proposed models for the dynamics of sand piles [8].

By pouring a granular material such as sand on a flat solid surface one ends up constructing a conical heap. Here we investigate what happens right after the poured sand hits the surface. We focus on the initial stages of an impacting jet of sand onto a flat surface and uncover the details of the dynamic patterns formed. Indeed, when a sand column falling from a funnel-shaped container, placed at a height H , impacts a flat solid surface, it fragments and gives rise to a fast radial flow outwards from the impact point. Right after impact, a thick initial ring forms which decelerates as it moves out from the center and eventually comes to a stop. The outgoing flux of particles starts to accumulate at the stopping point and an advancing ring-like sharp sand front forms. This front is the physical separation between the thin layer of flowing sand and the accumulated static sand left behind the front. Figure 1a shows a global view of this phenomenon with the impinging jet in the middle giving rise to the fast radial

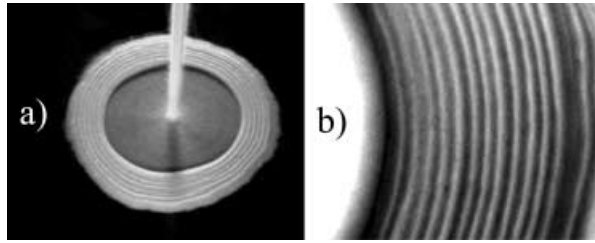


Fig. 1 – Photographs showing some of the main features of the impact of a granular jet on a smooth solid surface. a) A view from above showing the column or jet of sand at the center and the surrounding pattern showing signs of ripples on the outer annulus. The diffuse region between the jet and this outer region corresponds to the fast outgoing radial flow; b) a close up of the ripples on the outer annulus.

flow region and the surrounding annular region formed by the deposited sand left behind the front. Figure 1b is a close up on the outer region showing well-defined ripples. As the circular pattern closes, the sand front moving towards the injection point shows a periodic behavior: both the slope at the front and the velocity of this front as it advances change in time almost periodically. Along with this periodic behavior, the surface of the sand left behind the front shows the formation of ripples (see fig. 1b) which is directly correlated to the variations of the front angle and velocity. The formation of these ripples is very different from known ripple-forming situations where wind flow or water flow is at the origin of the observed ripples [1].

The experimental arrangement consists of different-size funnels used to pour the sand as a column; the diameter D of the funnel outlet controls the initial radius of the column and therefore the flux of sand. The solid surfaces used were made of glass (whose surfaces were optically smooth). The particles were glass beads with different diameters, 75 and 150 μm , but larger beads (450 μm) were also used in certain tests. We carried out the experiments for different heights H between funnel outlet and plate as this height controls the closing speed of the pattern. The experiments use video imaging both at a standard speed (25 images per second) and at faster rates (up to 1000 images/s). We used either a broad white light or a HeNe laser as light sources for the different visualizations we carried out. The laser beam was passed through a cylindrical lens to get a sheet of light for visualizing the sand front and its dynamics. In addition to varying the flux and the height of fall, we also tested this ripple formation on different substrates (roughened glass, metal, wood, and Plexiglas) to change the restitution coefficient and the friction coefficient between the grains and the plates. No variation was noted for different restitution coefficients (going from 0.5 to 0.8) and no variation as the roughness varied (we varied the friction coefficient from 0.25 to 0.4). We noted, however, that for rough surfaces, the ripples were generally ill defined. The friction coefficient was deduced from measurements of the position $r_f(t)$ of the first initial ring *vs.* time which could be fit by the expression: $r_f(t) = V_i t - \mu g t^2 / 2$, as if the assembly of grains were a solid block sliding on the substrate. V_i is the initial velocity right after impact, t is time after impact, μ is a friction coefficient (which is roughly constant *vs.* grain size from our experiments), and g is the gravitational acceleration.

A conspicuous feature of the patterns formed is the presence of ripples with a well-defined wavelength. The measured wavelengths are of order of a few millimeters and do not vary when the height of fall H changes. The size of the particles and the size of the funnel outlet D , on the other hand, modify the wavelength considerably. The variation of the wavelength with these two parameters is shown in fig. 2a which depicts the average wavelength *vs.* the funnel diameter for 3 different grain sizes at a fixed H . This figure shows that the wavelength

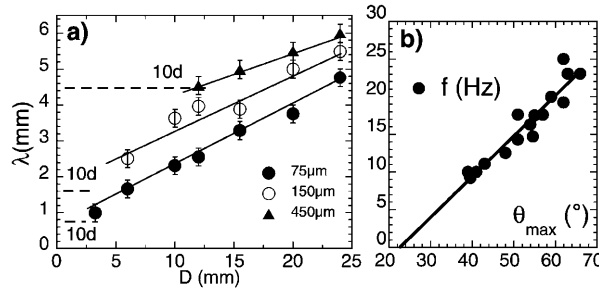


Fig. 2 – a) Variation of the wavelength of the ripples *vs.* funnel diameter D for three different bead diameters and a fixed height $H = 22.5$ cm; notice that there is a limiting wavelength below which no ripples are observed and which increases as the bead diameter increases. b) Variation of the frequency of the oscillations *vs.* the maximal angle at the front ($D = 12$ cm, $d = 75$ microns). The measurements were carried out for different heights of fall H ; both the frequency and the angle decrease with H .

increases linearly as the funnel diameter increases or as the flux increases; this wavelength also increases slightly as the grain size increases. There seems to be a wavelength, of about 10 grain diameters, below which no ripples are observed. When the ripple wavelength is only a few bead diameters, the ripples become very hard to observe. By measuring both the wavelength λ and the speed of closing V (which is constant for fixed H , D , and particle diameter d), we found that the characteristic frequency $\nu = V/\lambda$ of these oscillations is roughly constant and basically independent of the funnel diameter or flux (about 20 Hz and 15 Hz for the 75 and 150 μm particles, respectively at $H = 22.5$ cm). The velocity of the front and the wavelength both vary linearly with D giving a constant frequency. This frequency has also been measured independently and found to be similar to the one extracted from the velocity and the wavelength. Clearly, the existence of this characteristic time is at the heart of the ripple formation. While the wavelength is constant *vs.* H for a fixed flux, the frequency of the ripples decreases as H increases. The variation of H changes the maximal angle at the front which decreases as H increases. From measurements of the maximal angle at the front and the frequency *vs.* H , we found that the frequency increases roughly linearly *vs.* the maximal angle as seen in fig. 2b, a point to which we will come back below. The variation of H also changes the closing speed V which decreases as $H^{-0.66}$. These observations show that the three parameters, V , λ , and ν obey a linear dispersion relation, $V = \lambda\nu$ and scale, respectively, as $DH^{-0.66}$, D , and $H^{-0.66}$. The errors on the exponent are ± 0.1 . Thus the wavelength depends on D and therefore on the flux (which varies as $D^{2.5}$), while the characteristic frequency depends on the height of fall which modifies the maximal angle at the front. In the above scalings, we have neglected the dependence on the diameter of the beads which is relatively small.

More insight into the mechanisms leading to the formation of these ripples comes from a study of the local dynamics of the sand front associated with the closing of the ring as shown in fig. 3. Here a laser sheet is used to visualize the sand front. The sheet is perpendicular to the bottom plate and therefore to the ring itself and serves to visualize a line-like cut through the pattern in the radial direction r (the jet impact position corresponds to the origin). A typical time series of the front displacement is shown in fig. 3a and b, where we have split the rise and fall periods. As the front advances, one clearly sees variations of the front profile. The early time profile shows a roughly linear front with a small angle near the repose angle; as time elapses, the front angle increases and the height for a range of positions also increases (fig. 3a). Once the angle reaches a maximal value, an avalanche is generated, the angle decreases and the height for a range of positions r decreases indicating the onset of an avalanche (fig. 3b).

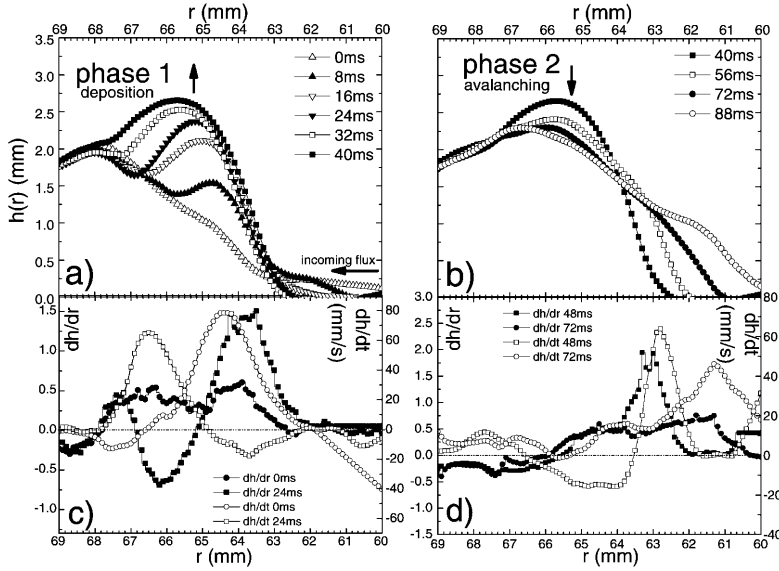


Fig. 3 – a) Evolution of the front profile at different times ($H = 17$ cm, $D = 12$ mm, $150 \mu\text{m}$ particles). The flow is from right to left while the front moves towards the right. For this figure we plot 6 successive profiles with a time step of 8 ms showing the deposition phase. b) Evolution of the following four profiles showing the avalanche phase. c), d) The temporal rate of change of the profiles and the spatial derivative of the profiles extracted from the profiles in a) and b) for two different times in the first phase (c) (deposition) and the second phase (d) (avalanching).

The angle can be relatively high compared with the angle of repose of a static sand pile. The variations of the angle can span a range between 30° and 65° . The repose angle of the beads ($150 \mu\text{m}$ beads) on the smooth glass substrate is about 20° . The position of the base of the front also changes periodically around the mean position as the front moves. The oscillations of the base position and the angle are out of phase: as the angle increases the position of the base lags behind the mean position, while when the angle decreases, the position of the base precedes the mean. By looking closely at the profiles, one notes that the position of the base of the front stays fixed, while the angle and the height right behind the front increase. As the base slips and moves the angle suddenly decreases and the height goes through a local minimum. This resembles a “stick-slip” type of motion. Along with these variations, a ripple is constructed on the sand surface as seen in fig. 3.

A simple argument in the framework of a model introduced recently [9,10], and which was found to describe sand fronts relatively well [6,7,11], helps to understand the formation of these ripples. This model was also used to understand aeolian ripples, but the presence of the hydrodynamic flow which interacts strongly with the sand layer renders it more complex [8,12]. The case we examine here is therefore much simpler and may allow for a better understanding of the nonlinear dynamics leading to ripple formation. An important element of this model is that the sand pile is considered to be made up of two layers, a static bottom layer of height h and an upper mobile layer of height R which includes the incoming flux in our case. The relation between these two variables, neglecting higher-order terms, is established through two coupled differential equations that read

$$\partial h(r,t)/\partial t = \alpha(r,t) - \gamma R(dh(r,t)/dr - C) = \Gamma(r,t) \quad (1)$$

and

$$\partial R(r, t)/\partial t = v_R(r, t)dR(r, t)/dr - \Gamma(r, t). \quad (2)$$

These two equations have a relatively simple meaning. The first one just says that the static layer increases at a rate $\alpha(r, t)$ by grains from the incoming flux of particles that get deposited along the front. This layer loses grains if its slope is higher than C ($= \tan\vartheta_r$, where ϑ_r is the repose angle). The second equation just states that the mobile layer is advected (up the slope or down the slope) with velocity v_R and changes at a rate $-\Gamma$.

A qualitative explanation of the observed front oscillations within the framework of this theory is as follows. The continuous sand flux arrives at the base of the front with a velocity V_0 (the velocity of the incoming flux of particles near the base of the front). This mobile sand of thickness R (of order of a few grains) then climbs up the slope of the front. A crucial issue is how this mobile sand gets deposited as this determines the shape of $\alpha(r, t)$. Here simple arguments suffice. This mobile layer decelerates as it climbs up (both gravity and friction contribute to this deceleration) so the higher it reaches the slower it moves. Near the summit the velocity of this mobile layer goes to zero. It is at locations between the summit and the base that deposition occurs; $\Gamma(r, t)$ is positive (so $\alpha(r, t)$ is positive at these positions) and the mobile-layer thickness R decreases. This deposition is more important at higher locations than near the base since the velocity decreases with the distance traveled. The grains will be deposited if their velocity is smaller than a threshold velocity as first noted by Bagnold [1]. The local slope dh/dr therefore changes and varies with position along the front. As this slope becomes sufficiently high (higher than the repose angle of the sand), static sand will be converted to mobile sand going down the slope (this is due to the second term in eq. (1)). The net deposition rate would then be the difference between the deposition coming from the mobile species going up the slope (given by the incoming flux) and the erosion through the mobile grains going down the slope. The complex interaction between these two opposing fluxes may also help deposition. A net decrease in the height of the static grains would occur when this difference is negative. An avalanche is then obtained. This avalanche will then erode the static part, reduce the local slope, and slow down in intensity. The angle becomes small and the whole cycle can then take place again. Of course, the maximum slope can be higher than the repose angle, since one needs a sufficient number of grains flowing down the slope to counterbalance the mobile grains going up the slope. A simple estimate of the maximal slope is given by $dh(r, t)/dr|_{\max} = \alpha(r, t)/\gamma R + C$. Now, the characteristic time mentioned above is directly related to an avalanche time between the maximal angle and the angle of repose, a problem that can be tackled in the framework of the above model as has been shown in ref. [13]. The avalanche time increases as the difference between the maximal angle and the angle of repose decreases according to the calculations of ref. [13]. Our measurements (fig. 2b) are in qualitative agreement with this latter statement. In addition, one can deduce that the ratio $\alpha(r, t)/\gamma R$ decreases as H increases (the frequency ν decreases *vs.* H). Also, since the frequency is independent of D (or the flux), the maximal angle stays the same *vs.* D and one can deduce that $\alpha(r, t)/\gamma R$ does not depend on the flux. Our measurements can therefore provide direct information on the parameters of the model.

In order to illustrate the qualitative explanation given above using the experimental data, we plot in fig. 3c and d the variation of h *vs.* time and the variation of the local slope (dh/dr). The first variation gives the total deposition or erosion rate Γ , while the second variation gives the local slope and therefore the contribution of the second term in eq. (1) which is responsible for avalanching. For the early time profile, the slope is near the repose angle and the deposition occurs mostly in a range of positions between the summit and the base as seen in fig. 3c. At a later time, the slopes where the initial deposition occurred have increased (see fig. 3c). The deposition now occurs farther up where the slopes are small. At positions where

the slopes are higher than the repose angle, erosion through avalanching occurs as indicated by the negative values of the rate of change of h as seen in fig. 3c. These observations are therefore consistent with the content of eq. (1). At even later times corresponding to the second phase (fig. 3b), erosion occurs at positions near the summit provoked by the high slopes at the base. Deposition occurs near the base where both the sand from the incoming flux and from the avalanching grains contribute to increase the local deposition rate. A fraction of the avalanching grains was also deposited behind the summit. Eventually, the slope becomes small through the avalanching process towards the base and the whole cycle can start all over again. The avalanche also increases the mobile-layer thickness as indicated by eq. (2), which then increases the influence of the second term in eq. (1). These observations are consistent with the above-mentioned model. The model being nonlinear however, its full resolution taking both the evolution in h and R into account is complicated but the simple case studied here can be a test bed for such coupled evolution equations. Another difficulty in applying this model stems from the high angles observed. The model is more suitable to angles near the repose angle which is true near the beginning of the deposition phase but not for the high angles observed near the end of this phase. It is more plausible to consider the high angles observed as a fluidized state and therefore as a dynamic rather than a static state. Here, estimates of the mobile layer are needed to go further and though our estimates indicate that R remains small, we have no proof that it does not vary markedly with the distance along the front. This is a three-dimensional problem and the visualization of the flowing layer is very difficult with simple photography. Our explanation is therefore only qualitative and further theoretical work is necessary to understand how to include these effects into the models available today.

In conclusion, we have presented new experimental observations and measurements on the impact of a granular jet on a flat solid surface. This gives rise to a circular sand pattern showing the formation of several ripples. These ripples form through oscillations of the sand front slope and speed. This is a novel way to construct ripples on sand as so far they are only seen when a hydrodynamic or aerodynamic flow exists above the sand bed. Our results may shed new light on the formation of ripples in general and on the interplay between deposition and avalanching which is important in a wide range of situations such as dune formation, sedimentation, and erosion.

REFERENCES

- [1] BAGNOLD R. A., *The Physics of Blown Sand and Desert Dunes* (Chapmann and Hall, Methuen, London) 1941.
- [2] JAEGER M., NAGEL S. R. and BEHRINGER R. P., *Rev. Mod. Phys.*, **68** (1996) 1259.
- [3] KADANOFF L. P., *Rev. Mod. Phys.*, **71** (1999) 435.
- [4] DE BRUYN J. R., BIZON C., SHATTUCK M. D., GOLDMAN D., SWIFT J. B. and SWINNEY H. L., *Phys. Rev. Lett.*, **81** (1998) 1421.
- [5] AMAROUCHENE Y., BOUDET J. F. and KELLAY H., *Phys. Rev. Lett.*, **86** (2002) 4286.
- [6] MAHADEVAN L. and POMEAU Y., *Europhys. Lett.*, **46** (1999) 595.
- [7] BONNIER B., BOUDET J. F. and KELLAY H., *Phys. Rev. E*, **68** (2003) 061302.
- [8] TERZIDIS O., CLAUDIN P. and BOUCHAUD J.-P., *Eur. Phys. J. B*, **5** (1998) 245.
- [9] BOUCHAUD J. P., CATES M. E., PRAKASH J. R. and EDWARDS S. F., *J. Phys. I*, **4** (1994) 1383.
- [10] BOUCHAUD J. P., CATES M. E., PRAKASH J. R. and EDWARDS S. F., *Phys. Rev. Lett.*, **74** (1995) 1982.
- [11] BOUDET J. F., GAUTHIER S., AMAROUCHENE Y. and KELLAY H., *Phys. Rev. E*, **67** (2003) 010303(R).
- [12] CSAHOK Z., MISBAH C., RIOUAL F. and VALANCE A., *Eur. Phys. J. E*, **3** (2000) 71.
- [13] BOUTREUX T. and DE GENNES P. G., *C.R. Acad. Sci. (Paris) Sér. II b*, **325** (1997) 85.